

Hyper-parallel Toffoli gate on three-photon system with two degrees of freedom assisted by single-sided optical microcavities

Hai-Rui Wei^{1,2*}, Fu-Guo Deng³ and Gui Lu Long^{1,2}

¹ School of Mathematics and Physics, University of Science and Technology Beijing, Beijing 100083, China

² State Key Laboratory of Low-Dimensional Quantum Physics and Department of Physics, Tsinghua University, Beijing 100084, China

³ Department of Physics, Applied Optics Beijing Area Major Laboratory, Beijing Normal University, Beijing 100875, China

[*hrwei@ustb.edu.cn](mailto:hrwei@ustb.edu.cn)

Abstract: Encoding qubits in multiple degrees of freedom (DOFs) of a quantum system allows less-decoherence quantum information processing with much less quantum resources. We present a compact and scalable quantum circuit to determinately implement a hyper-parallel controlled-controlled-phase-flip (hyper-C²PF) gate on a three-photon system in both the polarization and spatial DOFs. In contrast with the one with many qubits encoding in one DOF only, our hyper-C²PF gate operating two independent C²PF gates on a three-photon system with less decoherence, and reduces the quantum resources required in quantum information processing by a half. Additional photons, necessary for many approaches, are not required in the present scheme. Our calculation shows that this hyper-C²PF gate is feasible in experiment.

© 2021 Optical Society of America

OCIS codes: (270.0270) Quantum optics; (270.5585) Quantum information and processing; (270.5580) Quantum electrodynamics; (250.5590) Quantum-well, -wire and -dot devices.

References and links

1. M. A. Nielsen and I. L. Chuang, *Quantum Computation and Quantum Information* (Cambridge University, Cambridge, 2000).
2. F. Vatan and C. Williams, "Optimal quantum circuits for general two-qubit gates," *Phys. Rev. A* **69**, 032315 (2004).
3. G. Feng, G. Xu, and G. Long, "Experimental realization of nonadiabatic holonomic quantum computation," *Phys. Rev. Lett.* **110**, 190501 (2013).
4. Y. Liu, G. L. Long, and Y. Sun, "Analytic one-bit and CNOT gate constructions of general n-qubit controlled gates," *Int. J. Quantum Inf.* **6**, 447–462 (2008).
5. A. C. Santos and M. S. Sarandy, "Superadiabatic controlled evolutions and universal quantum computation," *Sci. Rep.* **5**, 15775 (2015).
6. M. Zwerger, H. J. Briegel, and W. Dür, "Hybrid architecture for encoded measurement-based quantum computation," *Sci. Rep.* **4**, 5364 (2014).
7. A. Reiserer, N. Kalb, G. Rempe, and S. Ritter, "A quantum gate between a flying optical photon and a single trapped atom," *Nature (London)* **508**, 237–240 (2014).
8. T. G. Tiecke, J. D. Thompson, N. P. de Leon, L. R. Liu, V. Vuletic, and M. D. Lukin, "Nanophotonic quantum phase switch with a single atom," *Nature (London)* **508**, 241–244 (2014).

9. Y. Y. Shi, "Both Toffoli and controlled-NOT need little help to universal quantum computing," *Quant. Inf. Comput.* **3**, 084–092 (2003).
10. E. Fredkin and T. Toffoli, "Conservative logic," *Int. J. Theor. Phys.* **21**, 219–253 (1982).
11. N. Yu, R. Duan, and M. Ying, "Five two-qubit gates are necessary for implementing the Toffoli gate," *Phys. Rev. A* **88**, 010304(R) (2013).
12. J. A. Smolin and D. P. DiVincenzo, "Five two-bit quantum gates are sufficient to implement the quantum Fredkin gate," *Phys. Rev. A* **53**, 2855 (1996).
13. A. Barenco, C. H. Bennett, R. Cleve, D. P. DiVincenzo, N. Margolus, P. Shor, T. Sleator, J. A. Smolin, and H. Weinfurter, "Elementary gates for quantum computation," *Phys. Rev. A* **52**, 3457 (1995).
14. J. Fiurášek, "Linear-optics quantum Toffoli and Fredkin gates," *Phys. Rev. A* **73**, 062313 (2006).
15. L. DiCarlo, J. M. Chow, J. M. Gambetta, L. S. Bishop, B. R. Johnson, D. I. Schuster, J. Majer, A. Blais, L. Frunzio, S. M. Girvin, and R. J. Schoelkopf, "Demonstration of two-qubit algorithms with a superconducting quantum processor," *Nature (London)* **460**, 240 (2009).
16. A. Fedorov, L. Steffen, M. Baur, M. P. da Silva, and A. Wallraff, "Implementation of a Toffoli gate with superconducting circuits," *Nature (London)* **481**, 170 (2012).
17. M. Hua, M. J. Tao, and F. G. Deng, "Fast universal quantum gates on microwave photons with all-resonance operations in circuit QED," *Sci. Rep.* **5**, 9274 (2015).
18. M. Hua, M. J. Tao, F. G. Deng, and G. L. Long, "One-step resonant controlled-phase gate on distant transmon qutrits in different 1D superconducting resonators," *Sci. Rep.* **5**, 14541 (2015).
19. H. R. Wei and F. G. Deng, "Scalable quantum computing based on stationary spin qubits in coupled quantum dots inside double-sided optical microcavities," *Sci. Rep.* **4**, 7551 (2014).
20. H. R. Wei and F. G. Deng, "Universal quantum gates on electron-spin qubits with quantum dots inside single-side optical microcavities," *Opt. Express* **22**, 593–607 (2014).
21. T. Monz, K. Kim, W. Hänsel, M. Riebe, A. Villar, P. Schindler, M. Chwalla, M. Hennrich, and R. Blatt, "Realization of the quantum Toffoli gate with trapped ions," *Phys. Rev. Lett.* **102**, 040501 (2009).
22. H. R. Wei and F. G. Deng, "Compact quantum gates on electron-spin qubits assisted by diamond nitrogen-vacancy centers inside cavities," *Phys. Rev. A* **88**, 042323 (2013).
23. D. Solenov, S. E. Economou, and T. L. Reinecke, "Fast two-qubit gates for quantum computing in semiconductor quantum dots using a photonic microcavity," *Phys. Rev. B* **87**, 035308 (2013).
24. B. P. Lanyon, M. Barbieri, M. P. Almeida, T. Jennewein, T. C. Ralph, K. J. Resch, G. J. Pryde, J. L. O'Brien, A. Gilchrist, and A. G. White, "Simplifying quantum logic using higher-dimensional Hilbert spaces," *Nat. Phys.* **5**, 134–140 (2009).
25. B. C. Ren, H. R. Wei, and F. G. Deng, "Deterministic photonic spatial-polarization hyper-controlled-not gate assisted by a quantum dot inside a one-side optical microcavity," *Laser Phys. Lett.* **10**, 095202 (2013).
26. B. C. Ren and F. G. Deng, "Hyper-parallel photonic quantum computation with coupled quantum dots," *Sci. Rep.* **4**, 4623 (2014).
27. B. C. Ren, G. Y. Wang, and F. G. Deng, "Universal hyperparallel hybrid photonic quantum gates with dipole-induced transparency in the weak-coupling regime," *Phys. Rev. A* **91**, 032328 (2015).
28. T. J. Wang and C. Wang, "Universal hybrid three-qubit quantum gates assisted by a nitrogen-vacancy center coupled with a whispering-gallery-mode microresonator," *Phys. Rev. A* **90**, 052310 (2014).
29. T. J. Wang, Y. Zhang, and C. Wang, "Universal hybrid hyper-controlled quantum gates assisted by quantum dots in optical double-sided microcavities," *Laser Phys. Lett.* **11**, 025203 (2014).
30. G. Vallone, G. Donati, R. Ceccarelli, and P. Mataloni, "Six-qubit two-photon hyperentangled cluster states: Characterization and application to quantum computation," *Phys. Rev. A* **81**, 052301 (2010).
31. D. Pile, "How many bits can a photon carry?" *Nature Photon.* **6**, 14–15 (2012).
32. E. Knill, R. Laflamme, and G. J. Milburn, "A scheme for efficient quantum computation with linear optics," *Nature (London)* **409**, 46–52 (2001).
33. K. Nemoto and W. J. Munro, "Nearly deterministic linear optical controlled-NOT gate," *Phys. Rev. Lett.* **93**, 250502 (2004).
34. Y. B. Sheng and L. Zhou, "Deterministic entanglement distillation for secure double-server blind quantum computation," *Sci. Rep.* **5**, 7815 (2015).
35. L. M. Duan and H. J. Kimble, "Scalable photonic quantum computation through cavity-assisted interactions," *Phys. Rev. Lett.* **92**, 127902 (2004).
36. C. Y. Hu, W. J. Munro, J. L. O'Brien, and J. G. Rarity, "Proposed entanglement beam splitter using a quantum-dot spin in a double-sided optical microcavity," *Phys. Rev. B* **80**, 205326 (2009).
37. H. R. Wei and F. G. Deng, "Scalable photonic quantum computing assisted by quantum-dot spin in double-sided optical microcavity," *Opt. Express* **21**, 17671–17685 (2013).
38. G. Balasubramanian, P. Neumann, D. Twitchen, M. Markham, R. Kolesov, N. Mizuochi, J. Isoya, J. Achard, J. Beck, J. Tisler, V. Jacques, P. R. Hemmer, F. Jelezko, and J. Wrachtrup, "Ultralong spin coherence time in isotopically engineered diamond," *Nat. Mater.* **8**, 383–387 (2009).
39. N. Bar-Gill, L. M. Pham, A. Jarmola, D. Budke, and R. L. Walsworth, "Solid-state electronic spin coherence time approaching one second," *Nat. Commun.* **4**, 1743 (2013).

40. G. D. Fuchs, V. V. Dobrovitski, D. M. Toyli, F. J. Heremans, and D. D. Awschalom, "Gigahertz dynamics of a strongly driven single quantum spin," *Science* **326**, 1520–1522 (2009).
41. T. Gaebel, M. Domhan, I. Popa, C. Wittmann, P. Neumann, F. Jelezko, J. R. Rabeau, N. Stavrias, A. D. Greentree, S. Prawer, J. Meijer, J. Twamley, P. R. Hemmer, and J. Wrachtrup, "Room-temperature coherent coupling of single spins in diamond," *Nat. Phys.* **2**, 408–413 (2006).
42. L. Robledo, L. Childress, H. Bernien, B. Hensen, P. F. A. Alkemade, and R. Hanson, "High-fidelity projective read-out of a solid-state spin quantum register," *Nature (London)* **477**, 574–578 (2011).
43. M. V. G. Dutt, L. Childress, L. Jiang, E. Togan, J. Maze, F. Jelezko, A. S. Zibrov, P. R. Hemmer, and M. D. Lukin, "Quantum register based on individual electronic and nuclear spin qubits in diamond," *Science* **316**, 1312–1316 (2007).
44. F. Shi, X. Rong, N. Xu, Y. Wang, J. Wu, B. Chong, X. Peng, J. Kniepert, R. S. Schoenfeld, W. Harneit, M. Feng, and J. Du, "Room-temperature implementation of the Deutsch-Jozsa algorithm with a single electronic spin in diamond," *Phys. Rev. Lett.* **105**, 040504 (2010).
45. T. van der Sar, Z. H. Wang, M. S. Blok, H. Bernien, T. H. Taminiau, D. M. Toyli, D. A. Lidar, D. D. Awschalom, R. Hanson, and V. V. Dobrovitski, "Decoherence-protected quantum gates for a hybrid solid-state spin register," *Nature (London)* **484**, 82–86 (2012).
46. S. Arroyo-Camejo, A. Lazarev, S. W. Hell, and G. Balasubramanian, "Room temperature high-fidelity holonomic single-qubit gate on a solid-state spin," *Nat. Commun.* **5**, 4870 (2014).
47. C. Zu, W. B. Wang, L. He, W. G. Zhang, C. Y. Dai, F. Wang, and L. M. Duan, "Experimental realization of universal geometric quantum gates with solid-state spins," *Nature (London)* **514**, 72–75 (2014).
48. E. Togan, Y. Chu, A. S. Trifonov, L. Jiang, J. Maze, L. Childress, M. V. G. Dutt, A. S. Sørensen, P. R. Hemmer, A. S. Zibrov, and M. D. Lukin, "Quantum entanglement between an optical photon and a solid-state spin qubit," *Nature (London)* **466**, 730–734 (2010).
49. H. Kosaka and N. Niikura, "Entangled absorption of a single photon with a single spin in diamond," *Phys. Rev. Lett.* **114**, 053603 (2015).
50. H. Bernien, B. Hensen, W. Pfaff, G. Koolstra, M. S. Blok, L. Robledo, T. H. Taminiau, M. Markham, D. J. Twitchen, L. Childress, and R. Hanson, "Heralded entanglement between solid-state qubits separated by three metres," *Nature (London)* **497**, 86–90 (2013).
51. C. Wang, Y. Zhang, R. Z. Jiao, and G. S. Jin, "Universal quantum controlled phase gates on photonic qubits based on nitrogen vacancy centers and microcavity resonators," *Opt. Express* **21**, 19252–19260 (2013).
52. H. R. Wei and G. L. Long, "Universal photonic quantum gates assisted by ancilla diamond nitrogen-vacancy centers coupled to resonators," *Phys. Rev. A* **91**, 032324 (2015).
53. B. C. Ren and F. G. Deng, "Hyperentanglement purification and concentration assisted by diamond NV centers inside photonic crystal cavities," *Laser Phys. Lett.* **10**, 115201 (2013).
54. N. B. Manson, J. P. Harrison, and M. J. Sellars, "Nitrogen-vacancy center in diamond: Model of the electronic structure and associated dynamics," *Phys. Rev. B* **74**, 104303 (2006).
55. J. R. Maze, A. Gali, E. Togan, Y. Chu, A. Trifonov, E. Kaxiras, and M. D. Lukin, "Properties of nitrogen-vacancy centers in diamond: The group theoretic approach," *New J. Phys.* **13**, 025025 (2011).
56. A. Batalov, V. Jacques, F. Kaiser, P. Siyushev, P. Neumann, L. J. Rogers, R. L. McMurtrie, N. B. Manson, F. Jelezko, and J. Wrachtrup, "Low temperature studies of the excited-state structure of negatively charged nitrogen-vacancy color centers in diamond," *Phys. Rev. Lett.* **102**, 195506 (2009).
57. D. F. Walls and G. J. Milburn, *Quantum Optics* (Springer-Verlag, Berlin, 1994).
58. J. H. An, M. Feng, and C. H. Oh, "Quantum-information processing with a single photon by an input-output process with respect to low-Q cavities," *Phys. Rev. A* **79**, 032303 (2009).
59. C. Y. Hu, A. Young, J. L. O'Brien, W. J. Munro, and J. G. Rarity, "Giant optical Faraday rotation induced by a single-electron spin in a quantum dot: Applications to entangling remote spins via a single photon," *Phys. Rev. B* **78**, 085307 (2008).
60. L. Zhou and Y. B. Sheng, "Complete logic Bell-state analysis assisted with photonic Faraday rotation," *Phys. Rev. A* **92**, 042314 (2015).
61. L. Zhou and Y. B. Sheng, "Detection of nonlocal atomic entanglement assisted by single photons," *Phys. Rev. A* **90**, 024301 (2014).
62. I. Fushman, D. Englund, A. Faraon, N. Stoltz, P. Petroff, and J. Vučković, "Controlled phase shifts with a single quantum dot," *Science* **320**, 769 (2008).
63. S. Sun, H. Kim, G. S. Solomon, and E. Waks, "A quantum phase switch between a single solid-state spin and a photon," *Nat. Nanotech.* **11**, 539 (2016).
64. P. E. Barclay, K. M. C. Fu, C. Santori, A. Faraon, and R. G. Beausoleil, "Hybrid nanocavity resonant enhancement of color center emission in diamond," *Phys. Rev. X* **1**, 011007 (2011).
65. P. Zhang, R. F. Liu, Y. F. Huang, H. Gao, and F. L. Li, "Demonstration of Deutsch's algorithm on a stable linear optical quantum computer," *Phys. Rev. A* **82**, 064302 (2010).
66. Y. B. Sheng, F. G. Deng, and G. L. Long, "Complete hyperentangled-Bell-state analysis for quantum communication," *Phys. Rev. A* **82**, 032318 (2010).
67. M. Scholz, T. Aichele, S. Ramelow, and O. Benson, "Deutsch-Jozsa algorithm using triggered single photons

- from a single quantum dot,” *Phys. Rev. Lett.* **96**, 180501 (2006).
68. R. Ceccarelli, G. Vallone, F. D. Martini, P. Mataloni, and A. Cabello, “Experimental entanglement and nonlocality of a two-photon six-qubit cluster state,” *Phys. Rev. Lett.* **103**, 160401 (2009).
 69. G. Vallone, G. Donati, N. Bruno, A. Chiuri, and P. Mataloni, “Experimental realization of the Deutsch-Jozsa algorithm with a six-qubit cluster state,” *Phys. Rev. A* **81**, 050302(R) (2010).
 70. D. G. England, K. A. G. Fisher, J. P. W. MacLean, P. J. Bustard, R. Lausten, K. J. Resch, and B. J. Sussman, “Storage and retrieval of THz-bandwidth single photons using a room-temperature diamond quantum memory,” *Phys. Rev. Lett.* **114**, 053602 (2015).
 71. R. Albrecht, A. Bommer, C. Deutsch, J. Reichel, and C. Becher, “Coupling of a single nitrogen-vacancy center in diamond to a fiber-based microcavity,” *Phys. Rev. Lett.* **110**, 243602 (2013).
 72. B. J. M. Hausmann, B. Shields, Q. Quan, P. Maletinsky, M. McCutcheon, J. T. Choy, T. M. Babinec, A. Kubanek, A. Yacoby, M. D. Lukin, and M. Lončar, “Integrated diamond networks for quantum nanophotonics,” *Nano Lett.* **12**, 1578–1582 (2012).
 73. J. Hagemeyer, C. Bonato, T. A. Truong, H. Kim, G. J. Beirne, M. Bakker, M. P. van Exter, Y. Luo, P. Petroff, and D. Bouwmeester, “H1 photonic crystal cavities for hybrid quantum information protocols,” *Opt. Express* **20**, 24714–24726 (2012).
 74. C. Bonato, E. van Nieuwenburg, J. Gudat, S. Thon, H. Kim, M. P. van Exter, and D. Bouwmeester, “Strain tuning of quantum dot optical transitions via laser-induced surface defects,” *Phys. Rev. B* **84**, 075306 (2011).
 75. L. C. Bassett, F. J. Heremans, C. G. Yale, B. B. Buckley, and D. D. Awschalom, “Electrical tuning of single nitrogen-vacancy center optical transitions enhanced by photoinduced fields,” *Phys. Rev. Lett.* **107**, 266403 (2011).
 76. K. M. C. Fu, C. Santori, P. E. Barclay, L. J. Rogers, N. B. Manson, and R. G. Beausoleil, “Observation of the dynamic Jahn-Teller effect in the excited states of nitrogen-vacancy centers in diamond,” *Phys. Rev. Lett.* **103**, 256404 (2009).
 77. A. Majumdar, E. D. Kim, and J. Vučković, “Effect of photogenerated carriers on the spectral diffusion of a quantum dot coupled to a photonic crystal cavity,” *Phys. Rev. B* **84**, 195304 (2011).
 78. P. Siyushev, H. Pinto, M. Vörös, A. Gali, F. Jelezko, and J. Wrachtrup, “Optically controlled switching of the charge state of a single nitrogen-vacancy center in diamond at cryogenic temperatures,” *Phys. Rev. Lett.* **110**, 167402 (2013).
 79. V. M. Acosta, C. Santori, A. Faraon, Z. Huang, K. M. C. Fu, A. Stacey, D. A. Simpson, K. Ganesan, S. Tomljenovic-Hanic, A. D. Greentree, S. Prawer, and R. G. Beausoleil, “Dynamic stabilization of the optical Resonances of single nitrogen-vacancy centers in diamond,” *Phys. Rev. Lett.* **108**, 206401 (2012).
 80. Y. Chu, N. P. de Leon, B. J. Shields, B. Hausmann, R. Evans, E. Togan, M. J. Burek, M. Markham, A. Stacey, A. S. Zibrov, A. Yacoby, D. J. Twitchen, M. Loncar, H. Park, P. Maletinsky, and M. D. Lukin, “Coherent optical transitions in implanted nitrogen vacancy centers,” *Nano Lett.* **14**, 1982–1986 (2014).
-

1. Introduction

Quantum computers promise to solve certain computational tasks which are intractable for a classical one [1]. Implementations of universal quantum logic gates, the central requirement for a quantum computer, have attracted widespread attention [2–6]. Much was focused on the two-qubit controlled-NOT (CNOT) gate or the identical controlled-phase-flip (CFP) gate [7, 8]. Multiqubit gates play a central role in quantum networks, quantum corrections, and quantum algorithms, and they serve as a stepping stone for implementing a scalable quantum computer. The simplest universal gate library in multiqubit systems is {Toffoli or Fredkin gate, Hadamard gate} [9, 10]. However, the inefficient synthesis [11, 12] of Toffoli or Fredkin gate increases the length and time of such two gates, and makes the gates further susceptible to their environments. The minimized cost of a three-qubit Toffoli gate is five two-qubit gates [11], and the decomposition of a generalized n -qubit Toffoli gate requires $O(n^2)$ two-qubit gates [13]. Some physical architectures, including linear optics, superconducting circuits, quantum dots (QDs), trapped ions, and diamond nitrogen-vacancy (NV) defect centres, have been proposed to implement Toffoli (or the identical C^2PF) gate with one degree of freedom (DOF) [14–22].

Quantum gates designed with minimized resources is crucial for quantum computation. Two strategies are generally adopted to remedy this problem: the one is to exploit a system with additional readily accessible states (qudit) during the computation [23, 24]; the second strategy is to encode the information in multiple DOFs of a quantum system. That is referred to as hyperparallel quantum gates [25–27], i.e., the quantum gates operating more than one independent

operations simultaneously. By the first approach, the quantum circuits for solid-state electronic CNOT gate [23] and flying photonic Toffoli gate [24] have been designed. By the second approach, schemes for implementing hyper-parallel photon-based CNOT gate [25–27] and hyper-parallel photon-matter-based universal gates [28, 29] have been proposed. The hyperentangled-cluster-state-based quantum computing have been demonstrated in recent years [30].

Single photon is one of the most popular candidates for quantum information processing with multiple DOFs because of its robustness against decoherence, exact and flexible manipulation with linear optics, and many accessible qubitlike DOFs [31], such as polarization, spatial, orbital angular momentum, transverse, energy-time, time bin, and so on. However, the photon-based quantum computing in a small-scalable fashion is a challenge in experiment because of the weak nonlinear interactions at the single-photon level. Fortunately, this intrinsic limitation can be partially solved by employing linear-optics [32] and completely solved by employing cross-Kerr nonlinearity [33, 34] or photon-matter entangling platforms [27, 35, 36]. Up to now, the giant Kerr nonlinearity is still a challenge in experiment. The mechanism of an emission-based photon-matter system can mediate a required photon-photon or matter-matter interaction, and opens up perspectives for directly photon-based [25, 26, 37], or matter-based [19, 20] scalable quantum computing in a determinate way. In addition, it allows the non-destructive photon-polarization (matter-spin) state measurement heralded by the states of the matter (photonic) qubit.

The electronic spins associated with the NV centre stand out as an attractive matter qubit because of their milliseconds coherence time [38, 39] and stable single-photon emission at room temperature, while can be manipulated on a subnanosecond time scale [40]. The exactly initialization [41], manipulation [40], and high-fidelity readout [42] of an NV centre electron spin, which is crucial for quantum information processing, have been reported in recent years. Nowadays, the NV centres have been subject to numerous applications: in 2007, Gurudev Dutt *et al.* [43] demonstrated distributed quantum computing in an NV centre. The Deutsch-Jozsa algorithm in a single NV centre was demonstrated in 2010 [44]. In 2012, van der Sar *et al.* [45] demonstrated the hybrid quantum gates acting on the electron spin and the nearby nuclear spin. In 2014, Arroyo-Camejo *et al.* [46] and Zu *et al.* [47] demonstrated geometric single-qubit gates and CNOT gate within an NV centre, respectively. In recent years, there have been a number of hallmark demonstrations of quantum entanglement between an emitted single photon and a stored NV centre electron spin (or between two separated NV centre spins) [48–50]. Based on NV-centre-emission-based entanglement, some interesting schemes for implementing universal gates on NV centre electronic [22] or photonic qubits [51, 52], and hyperentanglement purification and concentration were also proposed recently [53].

In this paper, we theoretically present an alternative scheme for compactly implementing an optical hyper- C^2 PF gate assisted by NV-centre-cavity systems. Our proposal has the following merits. First, single photons encoded in both the polarization and spatial DOFs, and this strategy reduces the quantum resource by a half than that with many qubits of one DOFs. Second, our universal gate works for a three-photon system in a hyper-parallel way. Third, additional photons, necessary for cross-Kerr- or parity-check-based photonic quantum computing, are not required. Fourth, our scheme is much simpler than that one cascaded with single- and two-qubit (CNOT or CPF) gates.

2. Compact quantum circuit for implementing hyper-parallel C^2 PF gate.

The NV centre consists of a substitutional nitrogen atom replacing a carbon atom and an adjacent vacancy in the diamond lattice. The ground states of the NV centre are an electronic spin-triplet state with a 2.88-GHz zero-field splitting between the magnetic sublevels with the angular momentum $m_s = 0$ and $m_s = \pm 1$ resulting from the spin-spin interactions [54]. The

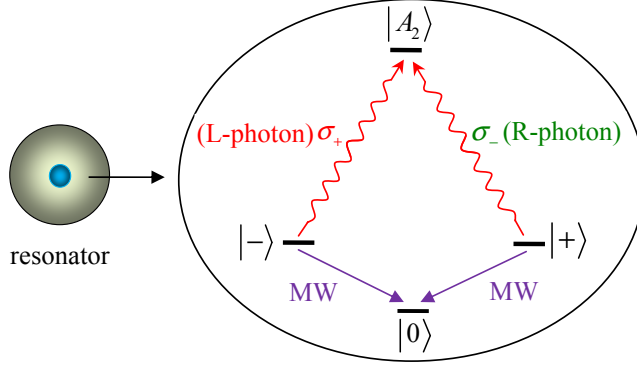


Fig. 1. A \wedge -type atom-like structure of the negatively-charged NV centre confined in an optical resonator. The states $|\pm\rangle$ act as the computational basis states, and the state $|0\rangle$ acts as an ancilla employed for spin manipulation. The optical transitions from the ground states $|\pm\rangle$ to the ancillary state $|A_2\rangle$ are coupled by the σ_{\mp} circularly polarized photons, respectively.

states $|m_s = \pm 1\rangle$ (denoted by $|\pm\rangle$) are coupled to the state $|m_s = 0\rangle$ (denoted by $|0\rangle$) with microwave pulses Ω_{\pm} forming a \vee -type three-level system. At low temperature ($T \approx 4$ K), the states $|\pm\rangle$ are coupled to one of the six excited states [55] $|A_2\rangle = (|E_{-}\rangle|+\rangle + |E_{+}\rangle|-\rangle)/\sqrt{2}$ with optical radiation forming a \wedge -type system [see Fig. 1]. The transitions $|\pm\rangle \rightarrow |A_2\rangle$ are driven by the σ_{\mp} polarized single photons at ~ 637 nm, respectively, and then the state $|A_2\rangle$ spontaneously decays into the states $|\pm\rangle$ with equal probabilities. Here $|E_{\pm}\rangle$ indicate the states with the angular momentum ± 1 along the NV centre axis, respectively. The state $|A_2\rangle$, an inherent spin-orbit entangled state and are protected by the spin-orbit and spin-spin interactions, is robust against the small strain and magnetic fields, preserving the polarization properties of its optical transition [56].

A diagram of a basic spin-photon entangling unit, a \wedge -type three-level NV centre trapped in a single-sided cavity, is shown in Fig. 1. An incident single photon with frequency ω_p enters a single-sided cavity with frequency ω_c . The cavity mode \hat{a} with the right and left circular polarizations, R and L , are resonantly coupled to the transitions $|\pm\rangle \rightarrow |A_2\rangle$ with frequency ω_0 , respectively. The cavity mode is driven by the input field \hat{a}_{in} . By solving the Heisenberg equations of motion for the annihilation operation \hat{a} of cavity mode and the lowering operation σ_{-} of the NV centre [57],

$$\begin{aligned} \frac{d\hat{a}}{dt} &= - \left[i(\omega_c - \omega_p) + \frac{\kappa}{2} \right] \hat{a}(t) - g\sigma_{-}(t) - \sqrt{\kappa}\hat{a}_{in}, \\ \frac{d\sigma_{-}}{dt} &= - \left[i(\omega_0 - \omega_p) + \frac{\gamma}{2} \right] \sigma_{-}(t) - g\sigma_z(t)\hat{a}(t) + \sqrt{\gamma}\sigma_z(t)\hat{b}_{in}(t), \end{aligned} \quad (1)$$

one [58, 59] can obtain the reflection coefficient for the NV-centre-cavity unit in the weak excitation limit $\langle \sigma_z \rangle = -1$,

$$r(\omega_p) = \frac{\hat{a}_{out}}{\hat{a}_{in}} = \frac{[i(\omega_c - \omega_p) - \frac{\kappa}{2}][i(\omega_0 - \omega_p) + \frac{\gamma}{2}] + g^2}{[i(\omega_c - \omega_p) + \frac{\kappa}{2}][i(\omega_0 - \omega_p) + \frac{\gamma}{2}] + g^2}. \quad (2)$$

Here, the cavity output field \hat{a}_{out} is connected with the input field \hat{a}_{in} by the input-output relation $\hat{a}_{out} = \hat{a}_{in} + \sqrt{\kappa}\hat{a}(t)$. $b_{in}(t)$, as the vacuum input field, has the standard commutation relation $[\hat{b}_{in}(t), \hat{b}_{in}^{\dagger}(t')] = \delta(t - t')$. γ is the decay rate of the NV centre population. κ is the damping

rate of the cavity intensity. σ_z is the inversion operator of the NV centre. g is the coupling rate of the NV-centre-cavity system.

From Eq. (2), one can see that if the single photon feels a hot cavity ($g \neq 0$), after reflection, it will get a phase shift $e^{i\varphi}$ with amplitude $|r(\omega_p)|$. If the photon feels a cold cavity ($g = 0$), after reflection, it will acquire a phase shift $e^{i\varphi_0}$ with amplitude $|r_0(\omega_p)|$. Considering the NV centre is prepared in the state $|+\rangle$, the R - (L -) polarized photon feels a hot (cold) cavity, and the corresponding state transformations are

$$\begin{aligned} |R\rangle|+\rangle &\rightarrow r(\omega_p)|R\rangle|+\rangle = e^{i\varphi}|r(\omega_p)||R\rangle|+\rangle, \\ |L\rangle|+\rangle &\rightarrow r_0(\omega_p)|L\rangle|+\rangle = e^{i\varphi_0}|r_0(\omega_p)||L\rangle|+\rangle. \end{aligned} \quad (3)$$

In case the NV centre electron spin is in the state $|-\rangle$, the corresponding transformations are

$$\begin{aligned} |R\rangle|-\rangle &\rightarrow r_0(\omega_p)|R\rangle|-\rangle = e^{i\varphi_0}|r_0(\omega_p)||R\rangle|-\rangle, \\ |L\rangle|-\rangle &\rightarrow r(\omega_p)|L\rangle|-\rangle = e^{i\varphi}|r(\omega_p)||L\rangle|-\rangle. \end{aligned} \quad (4)$$

Here r_0 is described by Eq. (2) with $g = 0$. The conditional phase shifts are the functions of the frequency detuning ($\omega_p - \omega_c$) under the resonant condition $\omega_c = \omega_0$. By adjusting $\omega_p = \omega_c = \omega_0$, it is possible to reach

$$r = \frac{-\kappa\gamma + 4g^2}{\kappa\gamma + 4g^2}, \quad r_0 = -1. \quad (5)$$

Ref. [58] shows that when $g \geq 5\sqrt{\gamma\kappa}$, $r(\omega_p) \simeq 1$. That is, the reflection of an uncoupled single photon can result in a phase shift π between the NV centre electron spin and the photon relative to the coupled one. The sign change of the reflected single photon can be specifically summarized as:

$$\begin{aligned} |R\rangle|+\rangle &\rightarrow |R\rangle|+\rangle, & |R\rangle|-\rangle &\rightarrow -|R\rangle|-\rangle, \\ |L\rangle|+\rangle &\rightarrow -|L\rangle|+\rangle, & |L\rangle|-\rangle &\rightarrow |L\rangle|-\rangle. \end{aligned} \quad (6)$$

The emitted photon-matter entangling platform is at the heart of the photon-based or matter-based scalable quantum computing [22, 52], Bell-state analysis [60], entanglement detection [61], and it has been received great progress in experiment. In 2008, Fushman *et al.* [62] observed phase shift $\pi/4$ in QD-cavity system. In 2014, Reiserer *et al.* [7] and Tiecke *et al.* [8] observed phase shift π in atom-cavity system. In 2016, Sun *et al.* [63] observed phase shift π in QD-cavity system. In the following, we exploit the spin-selective optical transition property described by Eq. (6) to study the implementation of the multi-photon hyper-parallel quantum computing.

Figure 2 depicts a compact quantum circuit for determinately implementing a hyper- C^2 PF gate acting on a three-photon system in both the polarization and spatial DOFs. This gate independently operates two C^2 PF gates simultaneously on a three-photon system. The C^2 PF gate is equivalent to the Toffoli gate up to two Hadamard transformations, i.e., $U_{C^2PF} = (I_4 \otimes H)U_{\text{Toffoli}}(I_4 \otimes H)$. Here I_4 is a 4×4 identity matrix and H represents the Hadamard operation performed on the target qubit. Let us assume that the single photons a , b , and c are initially prepared in the normalized states

$$\begin{aligned} |\varphi\rangle_a &= (\alpha_1|R_1\rangle + \alpha_2|L_1\rangle) \otimes (\zeta_1|a_1\rangle + \zeta_2|a_2\rangle), \\ |\varphi\rangle_b &= (\beta_1|R_2\rangle + \beta_2|L_2\rangle) \otimes (\zeta_1|b_1\rangle + \zeta_2|b_2\rangle), \\ |\varphi\rangle_c &= (\delta_1|R_3\rangle + \delta_2|L_3\rangle) \otimes (\xi_1|c_1\rangle + \xi_2|c_2\rangle). \end{aligned} \quad (7)$$

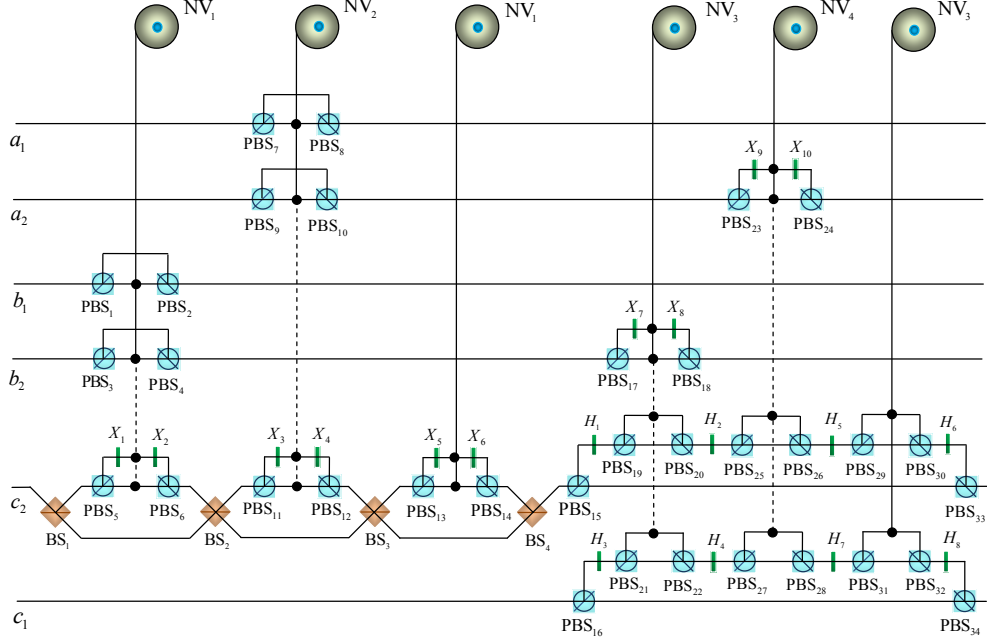


Fig. 2. Compact quantum circuit for implementing hyper-parallel C^2PF gate on a three-photon system with both the spatial and polarization DOFs. $CPBS_i$ ($i = 1, 2, \dots, 34$) represents a circular polarizing beam splitter that transmits the right circular polarizations (R) and reflects the left circular polarizations (L). H_i ($i = 1, 2, \dots, 8$) represents a Hadamard operation performed on the passing photon with a half-wave plate oriented at 22.5° . X_j ($j = 1, 2, \dots, 10$) represents a bit-flip operation performed on the passing photon with a half-wave plate oriented at 45° . BS_k ($k = 1, 2, 3, 4$) is a balanced polarization-preserving beam splitter.

The four NV centres, $NV_{1,2,3,4}$, with nearly identical electron-spin energy levels are respectively prepared in the states

$$|\varphi\rangle_{e_{1,3}} = \frac{|+1,3\rangle + |-1,3\rangle}{\sqrt{2}}, \quad |\varphi\rangle_{e_{2,4}} = \frac{|+2,4\rangle - |-2,4\rangle}{\sqrt{2}}. \quad (8)$$

Here, a_1 (b_1 or c_1) and a_2 (b_2 or c_2) are the two spatial modes of the photon a (b or c). R_1 (L_1), R_2 (L_2), and R_3 (L_3) denote the photon a , b , or c are in the right (left) circular polarization states, respectively. The subscript j of the $|+j\rangle$ ($|-j\rangle$) represents the j -th NV centre is in the state $|+\rangle$ ($|-\rangle$).

Now, let us go into the detail of our scheme in step by step for implementing the hyper- C^2PF gate.

First, photon b passes through the block $[PBS_1 \rightarrow NV_1 \rightarrow PBS_2$ or $PBS_3 \rightarrow NV_1 \rightarrow PBS_4]$. Subsequently, a Hadamard transformation H_{NV_1} is performed on NV_1 by applying a $\pi/2$ microwave pulse, which completes the transformations:

$$|+\rangle \rightarrow \frac{1}{\sqrt{2}}(|+\rangle + |-\rangle), \quad |-\rangle \rightarrow \frac{1}{\sqrt{2}}(|+\rangle - |-\rangle). \quad (9)$$

Here, PBS_i ($i = 1, \dots, 4$) is the circularly polarizing beam splitter which lets the component R of the incident photon be transmitted, while having the component L be reflected. The operations

(PBS₁ → NV₁ → PBS₂ → H_{NV₁} and PBS₃ → NV₁ → PBS₄ → H_{NV₁}) transform the total state of the system composed of photons a , b , c , and NV_{1,2,3,4} from $|\varphi_0\rangle$ to $|\varphi_1\rangle$. Here

$$|\varphi_0\rangle = |\varphi\rangle_a \otimes |\varphi\rangle_b \otimes |\varphi\rangle_c \otimes |\varphi\rangle_{e_1} \otimes |\varphi\rangle_{e_2} \otimes |\varphi\rangle_{e_3} \otimes |\varphi\rangle_{e_4}, \quad (10)$$

$$|\varphi_1\rangle = |\varphi\rangle_a \otimes |\varphi\rangle_c \otimes |\varphi\rangle_{e_2} \otimes |\varphi\rangle_{e_3} \otimes |\varphi\rangle_{e_4} \otimes (\zeta_1|b_1\rangle + \zeta_2|b_2\rangle) \otimes (\beta_1|R_2\rangle|-1\rangle + \beta_2|L_2\rangle|+1\rangle). \quad (11)$$

Second, photon c emitting from the spatial mode c_2 passes through the block [BS₁ → PBS₅ → X₁ → NV₁ → X₂ → PBS₆ → BS₂]. These operations make $|\varphi_1\rangle$ be changed into

$$|\varphi_2\rangle = |\varphi\rangle_a \otimes |\varphi\rangle_{e_2} \otimes |\varphi\rangle_{e_3} \otimes |\varphi\rangle_{e_4} \otimes (\zeta_1|b_1\rangle + \zeta_2|b_2\rangle) \otimes (\delta_1|R_3\rangle + \delta_2|L_3\rangle) \otimes [\beta_1|R_2\rangle(\xi_1|c_1\rangle - \xi_2|c_3\rangle)|-1\rangle + \beta_2|L_2\rangle(\xi_1|c_1\rangle + \xi_2|c_2\rangle)|+1\rangle]. \quad (12)$$

Here, $X_{1,2}$ represent the bit-flip operations performed on the passing photon with the half-wave plates oriented at 45°, i.e., $|R\rangle \leftrightarrow |L\rangle$. The balanced nonpolarizing beam splitter (BS), say BS₁ (BS₂), on the spatial states $|c_2\rangle$ and $|c_3\rangle$ is defined as

$$|c_2\rangle \rightarrow \frac{1}{\sqrt{2}}(|c_2\rangle + |c_3\rangle), \quad |c_3\rangle \rightarrow \frac{1}{\sqrt{2}}(|c_2\rangle - |c_3\rangle). \quad (13)$$

Third, photon a is injected into the block [PBS₇ → NV₂ → PBS₈ or PBS₉ → NV₂ → PBS₁₀], followed with an H_{NV₂} performed on NV₂. These operations (PBS₇ → NV₂ → PBS₈ → H_{NV₂} and PBS₉ → NV₂ → PBS₁₀ → H_{NV₂}) transform $|\varphi_2\rangle$ into

$$|\varphi_3\rangle = (\zeta_1|a_1\rangle + \zeta_2|a_2\rangle) \otimes (\zeta_1|b_1\rangle + \zeta_2|b_2\rangle) \otimes (\delta_1|R_3\rangle + \delta_2|L_3\rangle) \otimes (\alpha_1|R_1\rangle|+2\rangle + \alpha_2|L_1\rangle|-2\rangle) \otimes [\beta_1|R_2\rangle(\xi_1|c_1\rangle - \xi_2|c_3\rangle)|-1\rangle + \beta_2|L_2\rangle(\xi_1|c_1\rangle + \xi_2|c_2\rangle)|+1\rangle] \otimes |\varphi\rangle_{e_3} \otimes |\varphi\rangle_{e_4}. \quad (14)$$

Fourth, photon c emitting from the spatial mode c_2 or c_3 passes through the block [PBS₁₁ → X₃ → NV₂ → X₄ → PBS₁₂] and the block [BS₃ → PBS₁₃ → X₅ → NV₁ → X₆ → PBS₁₄ → BS₄] successively. After these two blocks, the state of the whole system becomes

$$|\varphi_4\rangle = (\zeta_1|a_1\rangle + \zeta_2|a_2\rangle) \otimes (\zeta_1|b_1\rangle + \zeta_2|b_2\rangle) \otimes (\delta_1|R_3\rangle + \delta_2|L_3\rangle) \otimes \{ \alpha_1|R_1\rangle|+2\rangle(\beta_1|R_2\rangle|-1\rangle + \beta_2|L_2\rangle|+1\rangle)(\xi_1|c_1\rangle + \xi_2|c_2\rangle) + \alpha_2|L_1\rangle|-2\rangle[\beta_1|R_2\rangle|-1\rangle(\xi_1|c_1\rangle + \xi_2|c_2\rangle) + \beta_2|L_2\rangle|+1\rangle(\xi_1|c_1\rangle - \xi_2|c_2\rangle)] \} \otimes |\varphi\rangle_{e_3} \otimes |\varphi\rangle_{e_4}. \quad (15)$$

Fifth, photon b in the spatial mode b_2 passes through the block [PBS₁₇ → X₇ → NV₃ → X₈ → PBS₁₈], followed by an H_{NV₃} performed on NV₃. The above operations (PBS₁₇ → X₇ → NV₃ → X₈ → PBS₁₈ → H_{NV₃}) transform $|\varphi_4\rangle$ into

$$|\varphi_5\rangle = \{ \alpha_1|R_1\rangle|+2\rangle(\beta_1|R_2\rangle|-1\rangle + \beta_2|L_2\rangle|+1\rangle)(\xi_1|c_1\rangle + \xi_2|c_2\rangle) + \alpha_2|L_1\rangle|-2\rangle[\beta_1|R_2\rangle|-1\rangle(\xi_1|c_1\rangle + \xi_2|c_2\rangle) + \beta_2|L_2\rangle|+1\rangle(\xi_1|c_1\rangle - \xi_2|c_2\rangle)] \} \otimes (\zeta_1|a_1\rangle + \zeta_2|a_2\rangle) \otimes (\zeta_1|b_1\rangle|+3\rangle + \zeta_2|b_2\rangle|-3\rangle) \otimes (\delta_1|R_3\rangle + \delta_2|L_3\rangle) \otimes |\varphi\rangle_{e_4}. \quad (16)$$

Sixth, after photon c passes through CPBS₁₅ (CPBS₁₆), the L -polarized component passes through the block [PBS₁₉ → NV₃ → PBS₂₀] or the block [PBS₂₁ → NV₃ → PBS₂₂]. Before

and after the wave-packet interacts with such two blocks, a Hadamard operation H_p , which completes the transformations $|R\rangle \rightarrow (|R\rangle + |L\rangle)/\sqrt{2}$ and $|L\rangle \rightarrow (|R\rangle - |L\rangle)/\sqrt{2}$, is applied on it with the half wave-plates H_1 and H_2 (H_3 and H_4) oriented at 22.5° , respectively. The operations (CPBS₁₅ \rightarrow H_1 \rightarrow PBS₁₉ \rightarrow NV₃ \rightarrow PBS₂₀ \rightarrow H_2 and CPBS₁₆ \rightarrow H_3 \rightarrow PBS₂₁ \rightarrow NV₃ \rightarrow PBS₂₂ \rightarrow H_4) transform $|\varphi_5\rangle$ into

$$\begin{aligned} |\varphi_6\rangle = & \{ \alpha_1 |R_1\rangle |_{+2}\rangle (\beta_1 |R_2\rangle |_{-1}\rangle + \beta_2 |L_2\rangle |_{+1}\rangle) (\xi_1 |c_1\rangle + \xi_2 |c_2\rangle) \\ & + \alpha_2 |L_1\rangle |_{-2}\rangle [\beta_1 |R_2\rangle |_{-1}\rangle (\xi_1 |c_1\rangle + \xi_2 |c_2\rangle) + \beta_2 |L_2\rangle |_{+1}\rangle \\ & (\xi_1 |c_1\rangle - \xi_2 |c_2\rangle) \} \otimes (\varsigma_1 |a_1\rangle + \varsigma_2 |a_2\rangle) [\zeta_1 |b_1\rangle (\delta_1 |R_3\rangle + \delta_2 |R_3\rangle) |_{+3}\rangle \\ & + \zeta_2 |b_2\rangle (\delta_1 |R_3\rangle + \delta_2 |L_3\rangle) |_{-3}\rangle] \otimes |\varphi\rangle_{e_4}. \end{aligned} \quad (17)$$

Seventh, photon a in spatial mode a_2 passes through the block [CPBS₂₃ \rightarrow X_9 \rightarrow NV₄ \rightarrow X_{10} \rightarrow CPBS₂₄]. Subsequently, an H_{NV_4} is applied on NV₄. These operations transform $|\varphi_6\rangle$ into

$$\begin{aligned} |\varphi_7\rangle = & \{ \alpha_1 |R_1\rangle |_{+2}\rangle (\beta_1 |R_2\rangle |_{-1}\rangle + \beta_2 |L_2\rangle |_{+1}\rangle) (\xi_1 |c_1\rangle + \xi_2 |c_2\rangle) \\ & + \alpha_2 |L_1\rangle |_{-2}\rangle [\beta_1 |R_2\rangle |_{-1}\rangle (\xi_1 |c_1\rangle + \xi_2 |c_2\rangle) \\ & + \beta_2 |L_2\rangle |_{+1}\rangle (\xi_1 |c_1\rangle - \xi_2 |c_2\rangle) \} \otimes (\varsigma_1 |a_1\rangle |_{-4}\rangle + \varsigma_2 |a_2\rangle |_{+4}\rangle) \\ & \otimes [\zeta_1 |b_1\rangle (\delta_1 |R_3\rangle + \delta_2 |R_3\rangle) |_{+3}\rangle + \zeta_2 |b_2\rangle (\delta_1 |R_3\rangle + \delta_2 |L_3\rangle) |_{-3}\rangle]. \end{aligned} \quad (18)$$

Eighth, photon c passes through the blocks [PBS₂₅ \rightarrow NV₄ \rightarrow PBS₂₆ \rightarrow H_5 \rightarrow PBS₂₉ \rightarrow NV₃ \rightarrow PBS₃₀ \rightarrow H_6] or the blocks [PBS₂₇ \rightarrow NV₄ \rightarrow PBS₂₈ \rightarrow H_7 \rightarrow PBS₃₁ \rightarrow NV₃ \rightarrow PBS₃₂ \rightarrow H_8] successively, and the wave-packets of the photon c are mixed at PBS₃₃ (PBS₃₄). The above operations change the state of the whole system to be

$$\begin{aligned} |\varphi_8\rangle = & \{ \alpha_1 |R_1\rangle |_{+2}\rangle [(\beta_1 |R_2\rangle |_{-1}\rangle + \beta_2 |L_2\rangle |_{+1}\rangle) (\xi_1 |c_1\rangle + \xi_2 |c_2\rangle)] \\ & + \alpha_2 |L_1\rangle |_{-2}\rangle [\beta_1 |R_2\rangle (\xi_1 |c_1\rangle + \xi_2 |c_2\rangle) |_{-1}\rangle \\ & + \beta_2 |L_2\rangle (\xi_1 |c_1\rangle - \xi_2 |c_2\rangle) |_{+1}\rangle] \} \\ & \otimes \{ \varsigma_1 |a_1\rangle |_{-4}\rangle [(\zeta_1 |b_1\rangle |_{+3}\rangle + \zeta_2 |b_2\rangle |_{-3}\rangle) (\delta_1 |R_3\rangle + \delta_2 |L_3\rangle)] \\ & + \varsigma_2 |a_2\rangle |_{+4}\rangle [\zeta_1 |b_1\rangle (\delta_1 |R_3\rangle + \delta_2 |L_3\rangle) |_{+3}\rangle \\ & + \zeta_2 |b_2\rangle (\delta_1 |R_3\rangle - \delta_2 |L_3\rangle) |_{-3}\rangle] \}. \end{aligned} \quad (19)$$

Finally, we measure the spins of NV_{1,2,3,4} in the basis $\{|\pm'\rangle = (|+\rangle \pm |-\rangle)/\sqrt{2}\}$ to disentangle the NV centres. Subsequently, the classical feed-forward single-qubit operations, as shown in Tab. 1, are performed on the three outing photons to raise the success probability of our hyper-C²PF gate to 100% in principle. These operations result in a three-photon output state

$$\begin{aligned} |\varphi_9\rangle = & \{ (\alpha_1 \beta_1 |R_1\rangle |R_2\rangle + \alpha_1 \beta_2 |R_1\rangle |L_2\rangle + \alpha_2 \beta_1 |L_1\rangle |R_2\rangle) (\xi_1 |c_1\rangle + \xi_2 |c_2\rangle) \\ & + \alpha_2 \beta_2 |L_1\rangle |L_2\rangle (\xi_1 |c_1\rangle - \xi_2 |c_2\rangle) \} \\ & \otimes \{ (\varsigma_1 \zeta_1 |a_1\rangle |b_1\rangle + \varsigma_1 \zeta_2 |a_1\rangle |b_2\rangle + \varsigma_2 \zeta_1 |a_2\rangle |b_1\rangle) (\delta_1 |R_3\rangle + \delta_2 |L_3\rangle) \\ & + \varsigma_2 \zeta_2 |a_2\rangle |b_2\rangle (\delta_1 |R_3\rangle - \delta_2 |L_3\rangle) \}. \end{aligned} \quad (20)$$

Therefore, the total operations for a deterministic hyper-C²PF gate are completed. That is, the quantum circuit shown in Fig. 2 completes a hyper-parallel optical C²PF gate which independently changes the phase of the input states by π , that is, a sign change, if all qubits are in the states $|L_1 L_2 c_2\rangle$ or $|a_2 b_2 L_3\rangle$, and has no effect otherwise.

Table 1. The classical feed-forward operations on the photonic qubits to complete a full and deterministic hyper-C²PF gate conditioned on the outcomes of the NV centre spins. $\sigma_z = |R\rangle\langle R| - |L\rangle\langle L|$. Phase shifter π performed on the spatial mode a_1 (b_2) completes the transformation $|a_1\rangle \rightarrow -|a_1\rangle$ ($|b_2\rangle \rightarrow -|b_2\rangle$).

NV centres	classical feed-forward operation
$ -\frac{1}{4}\rangle$ ($ +\frac{1}{4}\rangle$)	phase shift π is performed on the spatial mode a_1 (no)
$ -\frac{1}{3}\rangle$ ($ +\frac{1}{3}\rangle$)	phase shift π is performed on the spatial mode b_2 (no)
$ -\frac{1}{2}\rangle$ ($ +\frac{1}{2}\rangle$)	σ_z is performed on photon 1 (no)
$ -\frac{1}{1}\rangle$ ($ +\frac{1}{1}\rangle$)	$-\sigma_z$ is performed on photon 2 (no)

3. The average fidelity of the hyper-C²PF gate

The coefficients of the reflection photons, described by Eq. (2), play an important role in constructing our hyper-C²PF gate. The imperfection in phase and amplitude of the reflection photons reduces the performance of our gate. Therefore, it is necessary to consider the feasibility of our gate, which can be evaluated by the fidelity of the final normalized states in the realistic case $|\varphi'_{\text{out}}\rangle$ relative to that in the ideal case $|\varphi_{\text{out}}\rangle$ averaged over all the input (output) states, that is,

$$\bar{F} = \frac{1}{(2\pi)^6} \int_0^{2\pi} d\alpha \int_0^{2\pi} d\beta \int_0^{2\pi} d\gamma \int_0^{2\pi} d\zeta \int_0^{2\pi} d\zeta \int_0^{2\pi} d\xi |\langle \psi_{\text{out}} | \psi'_{\text{out}} \rangle|^2. \quad (21)$$

Here $|\varphi_{\text{out}}\rangle$ is described by Eq. (19). Using the same argument as for $|\varphi\rangle$, $|\varphi'_{\text{out}}\rangle$ can be obtained by substituting Eqs. (3)-(4) for Eq. (6). Here, $\cos \alpha = \alpha_1$, $\sin \alpha = \alpha_2$, $\cos \beta = \beta_1$, $\sin \beta = \beta_2$, $\cos \gamma = \gamma_1$, $\sin \gamma = \gamma_2$, $\cos \zeta = \zeta_1$, $\sin \zeta = \zeta_2$, $\cos \zeta = \zeta_1$, $\sin \zeta = \zeta_2$, $\cos \xi = \xi_1$, and $\sin \xi = \xi_2$. By calculation, we find that the average fidelity of our hyper-C²PF gate, \bar{F} , as a function of $g/\sqrt{\kappa\gamma}$ can be depicted by the red solid curve in Fig. 3.

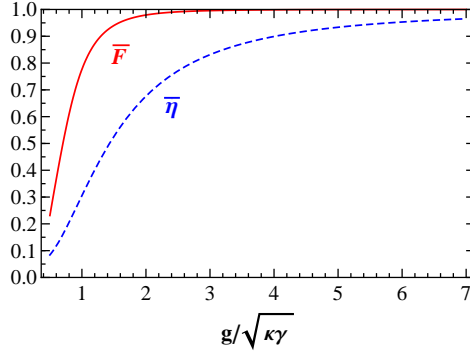


Fig. 3. The average fidelities (\bar{F} , red solid curve) and efficiencies ($\bar{\eta}$, blue dashed curve) of the hyper-C²PF gate as a function of $g/\sqrt{\kappa\gamma}$. $g/\sqrt{\kappa\gamma} \geq 0.5$.

4. The average efficiency of the hyper-C²PF gate

When the photon interacts with the matter qubit, the incident photon is inevitably lost. In order to show the feasibility of our gate, it is also necessary to consider the efficiency of our gate, η , which is defined as the yield of the incident photon, that is, the ratio of the gate's output photon

number n_{output} to its input photon number n_{input} . Taking all the possible input (output) states, that is, average over $\alpha, \beta, \gamma, \zeta, \xi \in [0, 2\pi]$, the average efficiency of our gate is given by

$$\begin{aligned}\bar{\eta} &= \frac{1}{(2\pi)^6} \int_0^{2\pi} d\alpha \int_0^{2\pi} d\beta \int_0^{2\pi} d\gamma \int_0^{2\pi} d\zeta \int_0^{2\pi} d\xi \frac{n_{\text{output}}}{n_{\text{input}}} \\ &= [121 + (128|r| + 164|r|^2 + 40|r|^3 + 14|r|^4 + |r|^5(2 + |r|)^2(4 + |r|)) \\ &\quad \times (91 + 58|r| + 42|r|^2 + 18|r|^3 + 12|r|^4 + 14|r|^5 + 14|r|^6 + |r|^7(6 + |r|))]/131072.\end{aligned}\tag{22}$$

The dependence of the average efficiency of our hyper-C²PF gate, $\bar{\eta}$, on the coupling strength $g/\sqrt{\kappa\gamma}$ is shown in Fig. 3 (see the blue dashed curve).

5. The challenges of our scheme.

In the work, the gate mechanism is deterministic in principle. However, the experimental imperfections degrade the gate fidelity and efficiency. The main sources of the errors include the finite signal-to-noise ratio in the zero-phonon line (ZPL) channel (reduces the fidelity of the platform by 11%) [48], the excited-state mixing caused by the strain and the depolarization of the single photons (reduces the fidelity of the platform by 12%) [48], timing jitter (reduces the fidelity of the platform by 4%) [48], spin-flips during the optical excitation result in the spin-spin interaction (probability $0.46 \pm 0.01\%$ when $T=4$ K) [50]. There are other errors due to the technical imperfections, such as imperfections in the NV centre electron spin population into state $m_s = 0$ (fidelity $99.7 \pm 0.1\%$) and states $m_s = \pm 1$ (fidelity $99.2 \pm 0.1\%$) [42], the imperfect rotations of the NV centre electron spin qubit by using microwave, the detector dark counts and background counts during the measurement of the NV centre, the spatial mismatch between the cavity and incident photon, the balancing of PBSs (extinction ratio about 100: 1 in reflection, 1000: 1 in transmission [7]) and BSs, and the intracavity loss and linear optical elements loss. The weak narrow-band ZPL emission at 637 nm is one the drawbacks of the applications of the NV centers, and about 70-80% of the NV centre's fluorescence emission is emitted into the narrow-band ZPL even at room temperature due to the low photon-electron coupling [64]. The imperfections due to the technical imperfection will be largely improved with the further technical advances.

6. Discussion and Summary

Optical quantum information processing has been received great attention and generally are focused on the traditional ones, in which the information is encoded in the polarization DOF of photons only. At variance with the traditional ones with one DOF, quantum information processing approach with multiple DOFs [65, 66] is much less affected by its environment, reduces the quantum sources, or can simplify one-way quantum computing and quantum algorithm [67–69]. Nowadays, hyper-parallel quantum gates have been recognized as an elementary element of quantum information processing. Some schemes for optical hyper-CNOT gates assisted by QDs or NV centres have been proposed by Ren *et al.* [25–27]. Wang *et al.* [28, 29] designed some quantum circuits for hyper-parallel universal quantum gates acting on hybrid photon-matter systems.

In this work, we have designed a compact quantum circuit for implementing an optical hyper-C²PF gate on a three-photon system in both the polarization and spatial DOFs through NV-centre-cavity interactions. Great efforts have been made to interact the NV centre with the photons. The single photon coupling to an NV centre electron spin has been reported in recent years [48, 49, 70]. An NV centre coupled to a fiber-based microcavity or microring resonator

has been demonstrated, respectively [71, 72]. A single NV centre coupled to a degenerate cavity mode, necessary for our scheme, can be achieved by employing the H1 photonic crystal cavity [73], fiber-based microcavity [71], ring microresonators [72], or micropillar [74]. The identically optical transition energies of the four separated NV centres, required for our scheme, can be achieved by applying controlled external electric fields [75]. Our scheme is nearly free from spectral diffusion and charge fluctuation [76] because of the narrow linewidth (40 MHz) of the state $|A_2\rangle$ [49]. The spectral diffusion, a hurdle for applications of the NV centres, is induced by a fluctuating electrostatic environment (usually caused by ionized impurities and charge traps) around the NV centre [77]. A number of techniques have been actively explored to reduce and eliminate the spectral diffusion [78–80].

In summary, we have presented a compact quantum circuit for implementing a three-photon hyper-parallel C^2PF gate with both the polarization and spatial DOFs, assisted by NV-centre-cavity interactions. Different from the traditional approach with encoding the qubit in polarization DOF of photons only, we encode the qubits in both the polarization and spatial DOFs of three photons, and our gate reduces the quantum resources consumed in quantum information processing by a half and the effect of the decoherence caused by the noise channels. In contrast to linear-optics- or parity-check-based procedures, our scheme does not require auxiliary single photons or maximally entangled pairs of photons. The cost is six CPF gates for our hyper- C^2PF gate. Given the current technology, our scheme may be experimentally feasible with a high fidelity and efficiency.

Acknowledgements

This work is supported by the National Natural Science Foundation of China (NSFC) (11547138, 11474026, 11175094 and 91221205), the Fundamental Research Funds for the Central Universities (06500024 and 2015KJJCA01), the National Basic Research Program of China (2011CB9216002). GLL is a member of the Center of Atomic and Molecular Nanosciences, Tsinghua University.